Global Change Biology (2003) **9,** 1643–1659, doi: 10.1046/j.1529-8817.2003.00690.x

# Detection of process-related changes in plant patterns at extended spatial scales during early dryland desertification

JORGE ARES, HÉCTOR DEL VALLE and ALEJANDRO BISIGATO
*National Patagonic Center, Boulevard Brown s/n, 9120 Puerto Madryn, Argentina*

**Abstract**

**Arid and semiarid shrublands occupy extensive land areas over the world, are susceptible to desertification by anthropic use and can contribute to regional climate change. These prompt the interest to monitor and evaluate these lands adequately in order to detect early stages of degradation. Evaluation topics must refer to biology-relevant characteristics of these systems, while simultaneously satisfying sampling consistency over extended landscape areas. We present an analysis of process-relevant parameters related to changes in the spatial arrangement of the plant canopy of shrublands inferred from high-resolution panchromatic aerial photos and Interferometric Synthetic Aperture Radar imagery. We obtained low-altitude images systematically located along several gradients of land-use intensity in a Patagonian Monte shrubland in Argentina. Images were digitized to spatial resolutions ranging from 0.09 to 0.72 m (pixel size) and the average values and an-isotropic characteristics of the plant canopy patterns were quantified by means of a Fourier metric. We used radar-derived imagery to overlay the panchromatic images on a digital elevation model in order to study the correspondence of potential runoff patterns and the spatial arrangement of plants. We related an-isotropic features of the plant canopy images to the prevailing wind regime. Observed trends were further interpreted on the basis of a spatial-explicit simulation model describing the dynamics of the main functional groups in the plant community. We conclude that early stages of anthropic-driven dryland degradation in the Patagonian Monte can be characterized by the incipient un-coupling of spatial vegetation patterns from those of runoff at a landscape scale, and a progressive coupling to the spatial pattern of the wind regime. The method and metrics we present can be used to quantify early desertification changes in other similar drylands at extended spatial scales.**

*Keywords:* desertification, drylands, Patagonia, remote sensing, spatial-explicit models, spatial vegetation patterns, wind erosion

*Received 22 October 2002; revised version received 16 April 2003 and accepted 26 June 2003*

## Introduction

Arid and semiarid drylands compose one-third of the land surface of the world (OIES, 1991). Among these, shrublands ($8.5 \times 10^6$ km$^2$) are fragile ecosystems prone to desertification (In what follows, 'desertification' implies a 'loss or spatial redistribution of net primary productivity in arid and semiarid lands' (Schlesinger *et al*., 1990).), as indicated in the case of the Mojave (Sharifi *et al*., 1999) and Chihuahuan (Schlesinger *et al*., 1990) systems in northern America and semiarid systems in central and southern Argentina (Busso, 1997). These systems share many structural and floristic characteristics (Mares *et al*., 1985).

The detection, prevention and/or adaptation to desertification and land degradation in general could benefit from improved monitoring methods (Reynolds *et al*., 2000). Monitoring shrublands in time to detect early deterioration is an unresolved subject in most cases. Most of our knowledge about the dynamics of these systems comes from relatively restricted

Correspondence: Jorge Ares, Cassila 76, 9120 Puerto Madryn, Argentina, fax + 54 2965 451021, e-mail: joares@arnet.com.ar

 

areas, including relatively small exclosures of major herbivores used to draw comparisons about their effect on the plant canopy (Brown & Waller, 1986). In many cases, the available knowledge has been obtained with techniques that are not amenable for use at a scale commensurate with the extension of drylands. Sometimes the interpretation of data can be limited by pseudoreplication effects imposed by the intensity of the sampling effort required in field observations of large terrestrial areas (Wester, 1992; Landsberg *et al*., 2002).

Identifying early desertification in shrublands also requires the selection of adequate 'signs', or relevant process-related parameters or monitorables to quantify the processes occurring at early stages of land degradation. Changes in the net primary production (NPP) have been indicated as conceptually adequate metrics (Schlesinger *et al*., 1990) and remote-sensing techniques have been applied to the analysis of the changes in time of aboveground NPP-related spectral vegetation characteristics in grazing gradients (Pickup *et al*., 1993, 1998). These experiences confirm that the aboveground NPP is a highly time-unstable characteristic of dryland ecosystems (Le Houérou *et al*., 1988). Interpreting its changes in time requires a detailed record of the highly variable precipitation events and the availability of suitable (i.e. day-time, cloud free, etc.) remotely sensed images some time (but in general shortly) after them. Unfortunately, quantitative multi-temporal arid region optical remote sensing is extremely difficult. In a recent review of the applications of optical satellite-based remote sensing, Okin (2001) concluded that despite their great promise, these methods have not yet proved capable of providing some types of information pertinent to desertification such as plant community composition.

Alternatively, the evaluation of changes of aboveground NPP (or surrogate indicators) in space seems to offer greater possibilities (Couteron & Lejeune, 2001; Okin, 2001). Low ($500 < \text{height} < 700$ m) aerial views of the vegetation in semiarid shrublands exhibit a spotted/banded pattern, where darker clumps or patches correspond to the shrub components interspersed on a background of lighter tones corresponding to open-space soil or herbaceous sparse vegetation.

There are numerous indications that the spatial distribution of vegetation in arid and semiarid lands is relevant to interpret basic ecosystem processes. The distribution of patches, their size and internal cover and the amount of denuded soil change in various proportions during shrubland deterioration by grazing or fire (Bisigato & Bertiller, 1997; Dunkerley, 1997; Adler *et al*., 2001). Consequently, with these, many functional characteristics related to water balance and fertility are modified, including or triggering losses of top soil, increased wind and water erosion, etc. (Beeskow *et al*., 1995; Schlesinger *et al*., 1996; Holm *et al*., 2001; Parizek *et al*., 2002). While these changes are measurable in labor-intensive field surveys, their detection by remote sensing would require a pixel resolution smaller than the scale of variability of the dominant elements (shrubs, grass tussocks, soil patches). This type of spatial resolution is not accessible in standard public-domain remote imagery, but *ad hoc* high-resolution aerial photographs can be used for this purpose (Hudak & Wessman, 1998).

Runoff patterns are closely related to the spatial structure of the plant canopy in drylands, as shown by Greene & Ringrose-Voase (1994) and Dunkerley & Brown (1999) in Australia, Galle *et al.* (1999) in Africa, Bergkamp *et al.* (1999) in Europe and Delhoumme (1996) in North America. Runoff patterns at a landscape scale ($>100$ m) can be estimated by means of standard statistical surface analysis techniques (Jenson & Domingue, 1996) applied to digital elevation models (DEM) based on InSAR (interferometric synthetic aperture radar**)** remote imagery (Coulson, 1995). This technique uses the phase information of a remote radar signal by taking the difference in path length (distance) from a given pixel on the Earth's surface to each SAR antenna. The phase difference for each pixel corresponding to the same area of the ground is known as an interferogram. Using the exact knowledge of the orbit parameters corresponding to the location of the remote sensor, the interferogram can be related directly to the altitude of the satellite above the ground on a pixel-by-pixel basis to generate a DEM. This is accomplished by combining two radar images of the same ground area taken from slightly differing orbiting angles.

In previous papers (Bertiller *et al*., 2002b; Ares *et al*., 2003a,b), we presented metrics derived from the Fourier spectral theory that allow inspection of high-resolution aerial photographs with the aim of detecting patterns in the structure of the plant canopy related to shrubland degradation by domestic grazing. The technique draws on results on the mechanisms through which sheep grazing impacts the structure of vegetation (Bisigato & Bertiller, 1997) and makes use of gray-palette aerial photography digitized to a spatial resolution of 1.5 m or less. Using this technique, and validating its estimates with field sheep fecal counts, long-term patterns of grazing use in the Patagonian Monte have been characterized. In large grazed paddocks with a single watering point located at one corner, both direct and inverse (bimodal) types of grazing gradients occur, but a direct trend (higher grazing pressure around watering points, diminishing at increasing distance from it) predominates when gradients of several paddocks are pooled in a regional

estimate. The possible reasons for the existence of inverse grazing gradients are the effect of nondomestic grazers excluded from sheep-visited areas, and the tendency of sheep to walk along the wind direction (Ares *et al*., 2003a).

In this study, we develop and further apply the technique to test its ability to quantify early stages of structural change in the plant community of drylands resulting from desertification mechanisms known to operate at a large spatial scale in domestic grazing systems in the southern Argentinian Monte. At these spatial scales, the detection of incipient structural changes is complicated by the occurrence of natural variability. Sheep grazing in the Patagonian Monte has been widespread during the last century, and no relict areas where a characterization of natural variability could be performed are now available. Spatial explicit modeling of shrub-grass plant canopies based on the changes observed in areas once intentionally denuded and in long abandoned fields supplied estimates of the spatial variability over large areas of the Patagonian Monte in terms of the above-mentioned Fourier metrics (Bisigato *et al*., 2002).

The emphasis in this paper is on the detection of subtle structural changes at large spatial scales as distinguished from approaches directed to evaluate severe changes at small spatial scales (dune formation, sand hummocks behind shrubs, deflation areas, etc.). In accordance with this approach, we selected an experimental system where desertification changes are not strikingly evident, but only sparsely distributed indications of its occurrence exist, like in localized deflation areas or small water channels barely distinguishable from naturally occurring bare soil patches or natural runoff rills. The overall question we address is: 'Can process-related metrics be developed that would quantify these minor changes at large spatial scales, where naturally occurring variability may mask their detection?'.

Specifically, we tested the following hypotheses:

1. In drylands lightly grazed by domestic herbivores (sheep) there is a component of large-scale spatial vegetation patterns related to the long-term pattern of herbivore use.
2. During early dryland degradation, the large-scale spatial vegetation pattern is progressively uncoupled from the landscape runoff system. This implies a diminishing correlation between plant canopy and runoff patterns as grazing impact increases.
3. During early desertification, the spatial vegetation pattern is progressively coupled to the pattern of the wind regime. This implies an increasing correlation between plant canopy and wind regime patterns as grazing impact increases.

We tested these hypotheses on a series of high-resolution aerial photographs along a transect in the southern Patagonian Monte in sites where previous field studies indicated the existence of sheep grazing gradients, and discuss the implications of the results for the identification and quantification of early stages of desertification in these and other similar drylands.

## Materials and methods

### *Description of the area*

Observations on the spatial arrangement of plant canopies were conducted in an area of about 300 $km^2$ centered at 42°38′S, 65°23′W in the southern Patagonian Monte (Chubut Province, Argentina, Fig. 1). The area selected is characteristic of the plain plateaus of gravels and the average annual rainfall (1975–1990) is 189 mm. Single precipitation events as high as 90 mm $day^{-1}$ have been recorded in this period, producing significant soil erosion, and intense showers are not rare. The vegetation is tall-shrub steppe of *Larrea* spp. characteristic of the southern portion of the Monte Phytogeographic Province, sharing floristic elements with the northern Patagonian Province (León *et al*., 1998). The vegetation is characteristic of the III Xeromorphic Tall Shrub floristic unit described in Ares *et al.* (1990) and


**Fig. 1** Location of the study site in South America, Argentina.

consists of patches of shrubs and perennial grasses, covering 40–60% of the soil. Sheep were introduced in the area at the beginning of last century (Defossé *et al.*, 1992) and are presently raised in large *estancias* (10000 ha or more), usually consisting in several paddocks around a shared watering place. In each paddock, gradients of land degradation produced by the concentration of sheep around watering places are common (Bisigato & Bertiller, 1997). Information about present and past sheep stocking rates, grazing pressures and/or grazing exclusion records are available for many paddocks during at least the last six decades. The Usual present grazing pressures in these paddocks range from 0.1 to 0.14 adult sheep $ha^{-1}$.

### *Field survey*

A set of aerial photographs (×36 exposures) from the fields were obtained on 29 May 2002 (morning flight, solar azimuth $+29^{\circ}$ to $+35^{\circ}$ clockwise from N)) with a regular auto-focusing 36 mm optical camera (Canon EOS 500N, Miami, FL, USA). The camera was mounted on the outside of the cabin of a two-seat ultra-light plane flying at 660 m above ground level, such that it would obtain nadir-oriented exposures when remotely triggered from the inside of the cabin. The field covered by a single exposure was estimated on the basis of a ground calibration of the exposure field in relation to the distance camera-object. Based on this, each exposure was estimated to cover a ground area of 1.8E4 $m^2$. After inspection of this photo-set, it became evident that testing Hypothesis 3 required obtaining new aerial images where the predominant wind direction would not overlap that of the sun-oriented plant shadows. Accordingly, a new photo-set was obtained during an afternoon flight on 31 July 2002 (solar azimuth: $-30^{\circ}$ to $-34^{\circ}$, anticlockwise from N).

The geo-positions at which photographs were obtained were previously selected on a geo-referenced LANDSAT TM composed image of the area. Target geo-positions were selected according to a systematic design involving three stages of domestic grazing impact as inferred from the distance to the local (property boundary) single watering point (Far: 4000–5000 m, Medium: 2000–3000 m, Near: <1000 m) in each of four paddocks at each of three *estancias* (Fig. 2). In this area, Bisigato & Bertiller (1997) found that sheep fecal counts, a surrogate indicator of local grazing intensity, increased by 40–60% in locations at 600 m from the water source, as compared with others at 3000 m from it, in paddocks where the average grazing pressure was 0.1–0.14 sheep $ha^{-1}$.

Target and realized geo-positions were linearly correlated (longitude $r^2 = 0.999$, latitude $r^2 = 0.994$), involving an estimated field geo-positioning error of ±150 m produced by small plane inclinations during flight.

### *Image digitizing and processing*

Negative exposure films (Kodak Color Film 100-7, Buenos Aires, Argentina) were converted to positive copies (150.2 × 101.0 mm). Copies were digitized to a gray palette (binary 8 bit $byte^{-1}$ integers, digital values: 0–255) with a desk-page scanner (Umax-Astra 3400 Fremont CA, USA) at resolutions 75, 150, 300 and

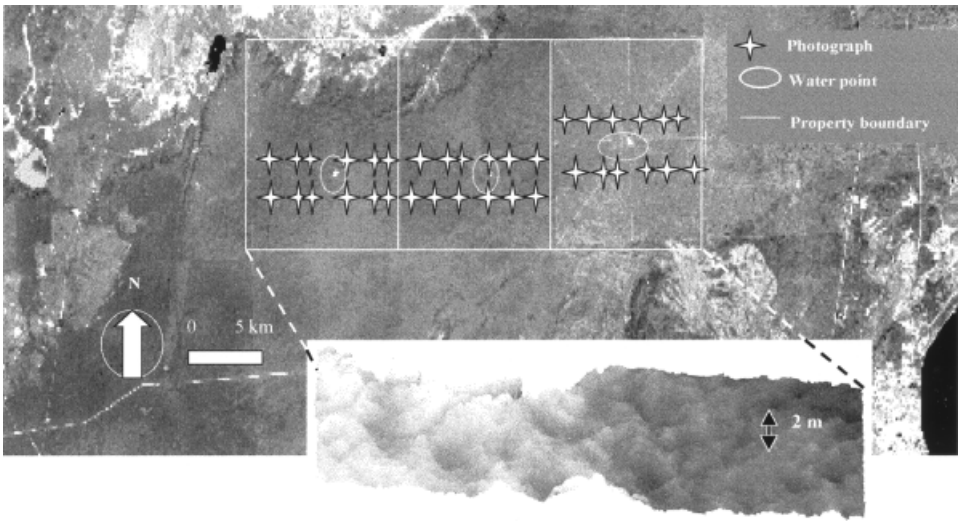


**Fig. 2** Flight plan and surveyed positions along a transect including three paddocks (*estancias*) at the Southern Patagonian Monte. The lower inset shows a 3-D view of the area with characteristic geomorphology patterns.

600 dpi. The scanning procedure resulted in gray-tone scaling proportional to shrub + grass cover on a lighter background corresponding to open soil patches. Several digitizing alternatives available were explored and discarded during preliminary trials either because they generated impractical large digital files at the desired resolution (real/true-color) noncontinuous (256 color) or bilateral-saturated file histograms (exposure autoscaling). Images were further inspected for sub-saturated value histograms, a necessary condition to prevent information loss. Image pixels thus obtained range from a spatial resolution of $0.09 \times 0.09$ m (600 dpi) to $0.72 \times 0.72$ m (75 dpi) in the field. Statistical tests in this study were applied to all resolution sets in order to avoid eventual artifacts in pattern inference due to the spatial resolution of the sampling procedure. Three square-windows, where the lateral size (in pixel units) satisfied the condition of being a power of 2, were extracted from each rectangular image in a systematic, nonoverlapping design (upper left, central, lower right). This size condition is a requisite for the application of the technique to characterize spatial patterns, which is explained in what follows.

We characterized the spatial pattern of vegetation by means of the Fourier signature *S/N*, (signal/noise ratio) developed in previous studies (Ares *et al.*, 2003a). The *S/N* metric refers to the spatial arrangement of a linear data vector, combining the evaluation of their departure from a random distribution, and the relative size of the 'peak' values along the data string. Anisotropy in spatial distribution can be evaluated by inspecting the variation of *S/N* ratios in data transects with diverse spatial orientation. The technique and some examples that illustrate the meaning of the *S/N* ratio are summarized in Appendix I. We wrote a computer code to calculate the *S/N* ratios corresponding to 20–30 randomly oriented transects in each photograph window.

### *Digital elevation model and potential runoff estimation*

We analyzed a sector (42°35′S–65°36′W to 42°41′S–65°06′W) of a digital elevation model (DEM) developed at the Remote Sensing Data Center (DFD) of the German Aerospace Center (DLR) and made available in the scope of this study (del Valle *et al.*, 2002). The DEM was computed on the basis of four ascending and one descending tandem from ERS/SAR 1-2 scenes with different interferometric baselines. Tandem data were selected based on usual criteria related to the coherence and baseline characteristics (Coulson, 1995). The horizontal DEM accuracy is 25 m, sampled at 1 m along the elevation axis.

Rasterized fields of potential runoff values (mm of water) (Jenson & Domingue, 1988) were computed over the area covered by the DEM, and local average values were computed for windows of $12 \times 12$ pixels ($300 \times 300$ m) centered at the estimated realized central geoposition of each photograph. The algorithm to calculate the potential runoff uses the information stored in the DEM, estimates local slopes and pixel orientations, and calculates the total amount of water potentially flowing through each image pixel in case all pixels would receive 1 mm of rain. Potential runoff is a surrogate estimate of actual runoff, since it can be expected that water will always flow along decreasing height gradients, although with different intensities depending on the intensity of the precipitation event.

### *Meteorological data*

#### *Analysis of spatial an-isotropy of the plant canopy in relation to the wind regime*

The average annual wind speeds and frequencies discriminated in 45°-azimuth sectors based on hourly averages observed during the period 1989–1998 at a station located on 42°46′S–65°02′W were obtained from the data bank of the Program of Environmental Physics, National Patagonic Center, Puerto Madryn. We defined wind intensities (*WI*):

$$WI_{i,j}\,(\mathrm{m\,s^{-1}}) = (\text{wind speed}_i\,(\mathrm{m\,s^{-1}}) \times \text{frequency}_i) - (\text{wind speed}_j\,(\mathrm{m\,s^{-1}}) \times \text{frequency}_j),$$

where $1<i<8$, $1<j<8$ refer to each of, respectively, opposite 45°-azimuth sectors in order to estimate the net effect of winds from opposite 45°-azimuth sectors on vegetation. The underlying assumption here is that the effect of winds from the SW could be partially reverted/masked by eventual posterior opposite winds from the NE, that from the W by those from E, etc. Since W–SW–S winds prevail in the area, we selected the subset of $WI>0$ and assigned them to northern ($-$ / $+$) azimuth values. The value corresponding to $WI_{W,E}$ is assigned to both the $-90$ and $+90$ azimuth positions, and intermediate WI values were estimated with nonlinear interpolation (Fig. 3).

We used the function:

$$S/N = f\,(WI) = a_0 + a_1 WI^4 + a_2 WI^3 + a_3 WI^2 + a_4 WI,$$

to describe the bi-modal effect of *WI* (note that *WI* is maximum at azimuth $+60°$ with a secondary local maximum at azimuth $-73°$). Analogously, we selected the function:

$$S/N = f\,(A) = b_0 + b_1 A^2 + b_2 A,$$

where $A$ is the transect azimuth to describe the unimodal apparent anisotropy produced by plant shadows.

(a)

**Wind regime**

**Annual average values**

| Sector | Frequency | Speed ($m/s^{-1}$) | Freq. X Speed |
|---|---|---|---|
| N | 0.064 | 6.1 | 0.3904 |
| NE | 0.132 | 5.1 | 0.6732 |
| E | 0.113 | 4.4 | 0.4972 |
| SE | 0.07 | 4.2 | 0.294 |
| S | 0.102 | 4.9 | 0.4998 |
| SW | 0.278 | 5 | 1.39 |
| W | 0.139 | 4.8 | 0.6672 |
| NW | 0.064 | 5.2 | 0.3328 |

| | Azimuth | WI |
|---|---|---|
| S–N | 0 | 0.1094 |
| SW–NE | 45 | 0.7168 |
| W–E | 90 | 0.17 |
| NW–SE | -45 | 0.0388 |
| E–W | -90 | 0.17 |

(b)

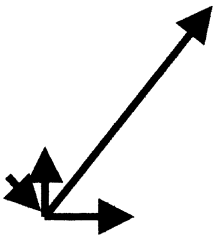

(c)

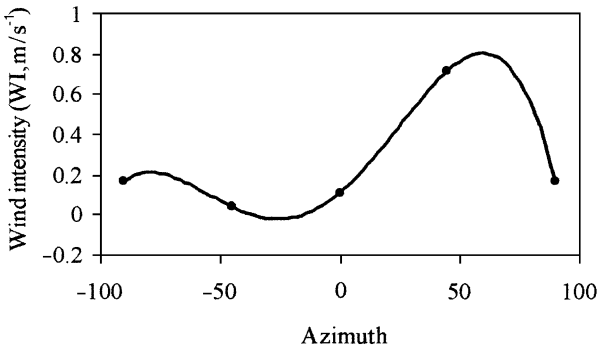


**Fig. 3** The average annual wind regime in the study area. (a) Frequencies, velocities and Wind Intensities (WI) pooled by 45°-azimuth sectors as defined in the text. (b) Discrete vector representation. (c) Continuous fitted function.

*Spatial simulation model*

In order to explore the numerical feasibility and internal consistency of the tested hypotheses about the dynamics of vegetation patterns, we used a previously developed (Bisigato *et al.*, 2002) spatial-explicit, difference equation, dynamic cellular automata model (Baker, 1989; Wiegand *et al.*, 1995). The model (*PATCHGEN*, Table 1, Fig. 4) simulates the development of vegetation canopies in Monte shrublands on the basis of a set of rules related to the allometry of shrubs and perennial grasses and the observed carrying capacity of relatively undisturbed field sites with respect to them. The growth of shrubs and perennial grasses is conceived as depending on the existent volume at each grid element and the volumes of plants of the same type diffusing to/from neighbor grid cells. An-isotropic growth can be introduced in the model at 45° intervals, by assuming different diffusive growth rates to cells in the octet surrounding each grid cell. Allometric descriptors of shrubs and grasses are introduced by assuming a frequency distribution of plant volume sizes similar to those observed in relatively undisturbed fields. Increasing runoff intensity reduces the potential plant size (carrying capacity) at each microsite, implying an increased local nutrient loss (Dunkerley & Brown, 1999). The effect of sheep grazing on the structure on the plant canopy is introduced by assuming that sheep select the most productive plant patches nearby before starting consumption at a next neighboring patch, moving to another grazing station when no neighbor patch offers biomass above a critical threshold level (Ares *et al.*, 2003a). The model generates several types of outputs, including Fourier analysis of random linear transects and raster grids compatible with display color palettes scaled as needed to mimic field aerial photographs at various spatial resolutions.

*Statistical analysis and numerical simulation*

Preliminary searches of spatial patterns in digitized field photographs and in model-output imagery were performed with software developed for percolation analysis (Milne *et al.*, 1999). The average grazing impact was assumed to be at a highest level at places near the watering sources, intermediate at mid-away positions and lighter at the farther positions (Fig. 2). The null Hypothesis 1 (no grazing effect upon plant spatial distribution) was tested by comparing the frequency distributions of *S/N* values at Far, Medium and Near positions (12 exposures × 20 transects × 4 spatial resolutions = 960 values/position) by means of a nonparametric $\chi^2$ test (Crow *et al.*, 1993).

The null hypothesis 2 (relation of vegetation pattern to runoff not depending on grazing impact) was tested by inspecting the linear correlation between the average *S/N* of exposures at Far, Medium and Near positions (dependent variable) with the corresponding average potential runoff values (independent variable). The linear correlation was selected as an estimate of Euclidean distance of the data points to a reference function, and parsimony search indicated that the fit did not improve for fitting functions of higher order. This, however, should not be interpreted *sensu stricto* to

**Table 1** Structure and algorithms in the shrubland spatial-explicit simulation model *PATCHGEN*

| Structure, process | Rule, algorithm |
|---|---|
| 1. Spatial organization, resolution | Grid of square (0.25 m × 0.25 m) cells. The dynamic behavior of each cell is assumed to depend on those of the surrounding octet. |
| 2. Numerical rationale, variables | Difference equations; time step: 1 week; random generator: Ansi C drand routine. Simulated variables: aboveground plant volumes ($cm^3$/cell) of shrubs and perennial grasses. |
| 3. Vegetation types simulated | Shrubs (S), perennial grasses (PG). |
| 4. Plant colonization | Isotropic random for S and PG during seed rain time, S with higher probability when neighbor cells already occupied by a big S, S with lower probability when cell already occupied by big PG. Alternatively, anisotropic depending on runoff and wind intensity. |
| 5. Potential local plant size | S and PG size class set at colonization time, depending on random selection from observed sizes in relatively undisturbed fields, modulated by runoff intensity at the colonized cell (higher potential runoff ⇒ smaller plant size). |
| 6. Plant local growth | S and PG growth based on maximum observed rates in juvenile plants, modulated by a seasonal factor depending on temperature and soil moisture average cycles and a maximum carrying capacity estimated from field data and runoff intensity. The implication is that increased runoff diminishes soil fertility, which in turn reduces the maximum possible size of both S and PG. |
| 7. Plant diffusional growth | A starter S or PG at one cell can expand to a randomly selected (out of 8) neighbor cells at each time step depending on a 'diffusional gradient' logic, where both the sum of S and PG at the receiving cell define the target side of the gradient. Anisotropy is introduced by assigning asymmetric diffusive coefficients to different orientations within the octet surrounding each grid cell. |
| 8. Plant competition | S and PG volumes at each cell constrained by a linear function of both and by maximum individual size set at colonization time. |
| 9. Grazing pattern | Grazers are assumed to optimize harvest effort by first consuming the most productive patch nearby and abandoning it as local yield decreases below local threshold. |

imply that a linear relation is proposed for the data (or the underlying process they describe), in fact any higher order function would have served the purpose of obtaining descriptors based on Euclidean distances to a reference function. Estimates at all spatial resolutions (12 windows × 4 resolutions × 3 positions = 144 average values) were used to build confidence intervals for the correlation coefficients by randomly sampling across resolutions according to a Monte Carlo procedure. The correlation estimates were then regressed against distance to the watering point and the most significant trend was identified along a new parsimonious search sequence.

Additionally, the consistency of a mechanistic explanation for the observed trend relating spatial patterns and runoff was tested with *PATCHGEN* by running the model on potential runoff surfaces corresponding to the sample photographed field areas.

The null hypothesis 3 (no anisotropy related to regional wind pattern) was tested on the photo-set obtained on 31 July 2002, since the solar azimuth tends to be perpendicular to *WI* directions during postmeridian time in the region of predominant westerly winds of the southern hemisphere. In this photo-set, plant solar shadows appear at an angle 70–75° with respect to the annual average predominant *WI*-azimuth. This enhances the ability of statistical tests to discriminate between apparent anisotropy in the aerial images produced by sun-shadow effects from eventual actual anisotropy produced by winds. The nonlinear correlation between *S*/*N* values at Far, Medium and Near positions (dependent variable) with *WI* and A were computed. Both functions were regressed jointly and separately as independent variables against the *S*/*N* values (dependent variable), in order to discriminate the magnitude of the an-isotropic effects associated to each of them.

Three windows (upper left, center, lower right) were sampled within each exposure. A total of 20 values/window × 12 exposures × 3 windows/exposure = 720 *S*/*N* values were used for each position in these analyses. An-isotropic effects were also simulated with *PATCHGEN* at the observed range of runoff values, by assuming that the lateral diffusive growth at each pixel

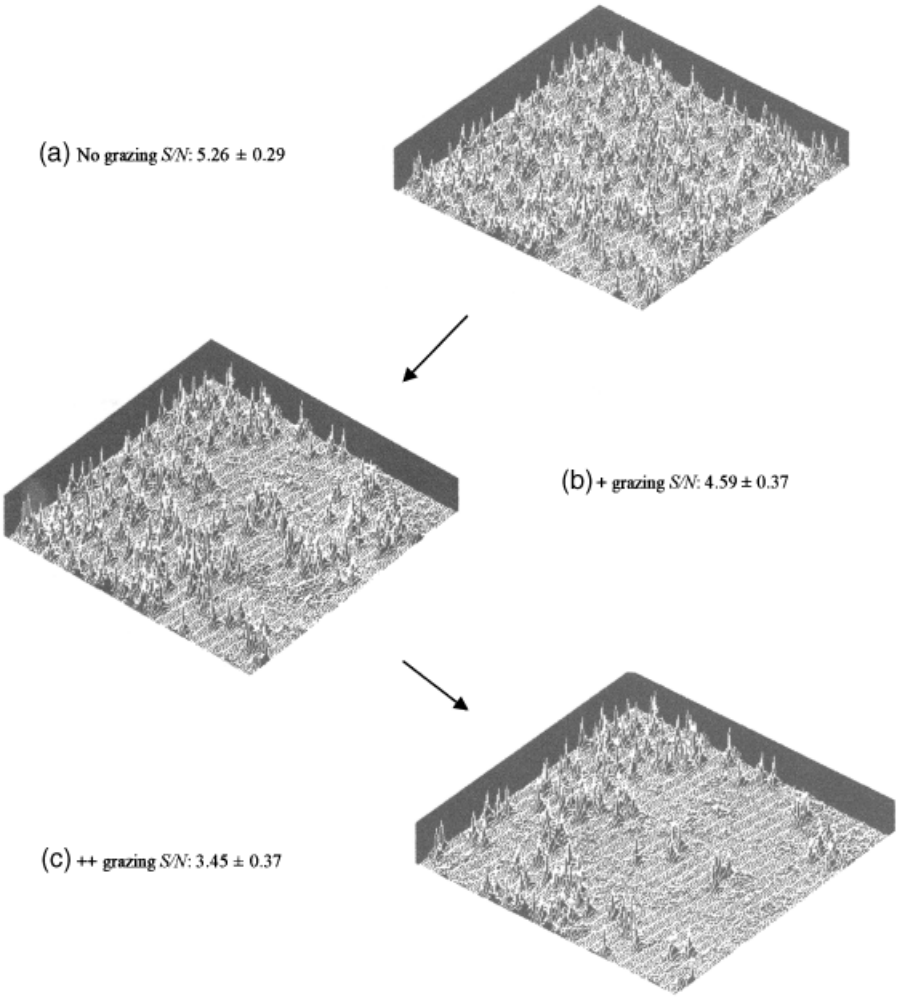


**Fig. 4** Sample realizations of the PATCHGEN model showing stages of patch growth and patterns of their destruction by 'optimal' herbivores. (a) Hypothetical predomestic grazing stage. This is created by assuming a net growth of randomly located patches under very light grazing; (b) Domestic grazing produces a stage of partial destruction of patches and reduction of their overall size and uniformity of their distribution; (c) Heavy grazing. A few patches remain at this stage, others are reduced in size and fragmented.

octet was proportionally related to the annual pattern of WI (see also Table 1).

## Results

### *Hypothesis 1: Grazing modifies the spatial pattern of the vegetation canopy*

Figure 5a and b shows a summary of the values of Fourier $S/N$ signatures describing the structure of the vegetation in the study area at spatial resolutions $0.09 \times 0.09$ m. The field data obtained as shown in Fig. 1 have been projected on a vertical plane centered at $-42.64$ S for ease of visualization. The arrows indicate the position of the areas where the water points are located and the dotted lines indicate the wire fences dividing the three paddocks sampled in this study (see also Fig. 2). The picture is equivalent to considering a lateral view of the study area, where the position of water points and paddock wire fences is also indicated. Note that data means, ranges and kurtoses show regular local lows in approximate coincidence with the location of water points (arrows). Other less marked local minima also occur along easterly wire-fences. These trends indicate that the large spatial (200–300 m) variability of the plant structure diminishes near water points (where fecal counts indicate a higher grazing intensity) or at places where sheep tend to concentrate during wind storms. Mechanisms that account for higher grazing intensity along easterly fence lines have been discussed in our previous study (Ares, 2003a) and include the tendency of sheep to walk along the wind

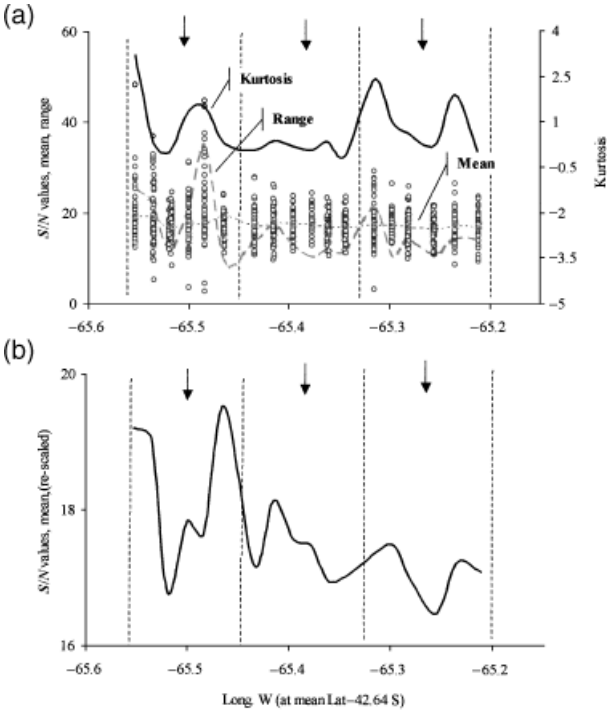


**Fig. 5** (a) Summary of the values of Fourier $S/N$ signatures describing the structure of the vegetation in the study area. The field data obtained as shown in Fig. 2 have been projected on a vertical plane centered at $-42.64$ S for ease of visualization. The arrows indicate the position of the areas where the water points are located and the dotted lines indicate the wire fences dividing the three paddocks sampled in this study. (b) Mean values in inset 'a' re-scaled to show detail.

direction and the behavioral-based exclusion of sheep and guanacos in the area. A local mean low at $-65.45$W probably results from the observed occurrence of a temporary water source east from the fence that sheep use to visit.

Table 2 shows an analysis of the histograms of the frequency distributions of these data as well as those obtained at resolutions $0.18 \times 0.18$ m, $0.36 \times 0.36$ m, $0.72 \times 0.72$ m. In this analysis, the data were further stratified according to the location of the corresponding photograph relative to the watering points (Near–Medium–Far). Significant differences between the frequency distribution at Far with respect to Near positions occur at all sampling resolutions. In other cases, there are also marked differences between Far–Medium and Medium–Near positions. The changes observed in the histograms corresponding to all sampling resolutions consist in the increase of the frequencies at the central range of $S/N$ values at the expense of lower-class values as distance to the water point decreases. Based on these results, we do not find reasons to reject the hypothesis that the large-scale

**Table 2** Results of $\chi^2$ tests of differences between histograms of frequency distributions of $S/N$ values corresponding to positions Near–Medium–Far relative to the nearest water source

| Spatial resolution (m) | Far–Near | Far–Medium | Medium–Near |
|---|---|---|---|
| $0.09 \times 0.09$ | **35.6** | **37.3** | **17.0** |
| $0.18 \times 0.18$ | **29.8** | 10.9 | 12.2 |
| $0.36 \times 036$ | **26.9** | **24.3** | 10.9 |
| $072 \times 0.72$ | **42.2** | 7.1 | **21.3** |

See also Figs 2 and 5. Values significant at $P < 0.05$ shown in bold.

spatial structure of the vegetation canopy is modified by the impact of grazing in the study area.

*Hypothesis 2: Diminishing correlation between plant canopy and landscape-scale runoff patterns as grazing impact increases*

Figure 6 shows images of two field areas representing extreme differences in estimated potential runoff, and their corresponding average $S/N$ and percolation metric values. Photograph 14 corresponds to a low-runoff, high-$S/N$ area Far from the water source, while photograph 7 is from a high-runoff, low-$S/N$ area Far from water source. See that a smoother texture predominates at photograph 7 in relation to photograph 14. This is confirmed by the lower average cluster size and higher number of clusters as estimated with percolation metrics. Figure 7a–c shows the results of the analyses of linear correlation relating image average $S/N$ values with the corresponding average potential runoff values in the area centered at their estimated realized geoposition, at Far–Medium–Near positions, based on all resolutions. Note that a significant correlation exists at the positions 'Far' that vanishes at 'Medium' and 'Near' positions. In order to test the null hypothesis ($r^2_{S/N}$ vs. Runoff vs. Distance to Water Point = 0), random sub-samples of the data in Fig. 7a–c were drawn by means of a Monte Carlo procedure in which $S/N$ estimates at each resolution were sequentially sampled from each group in order to generate estimates of $r^2_{S/N}$ vs. Runoff. The average $r^2$ values and their confidence intervals obtained by this procedure are shown in insets a–c and summarized in Fig. 7d. Based on the results in Fig. 7d, we found no reason to reject the hypothesis that the spatial vegetation structure as estimated through the $S/N$ metric is progressively un-coupled from the landscape runoff pattern at early stages of increasing grazing impact.

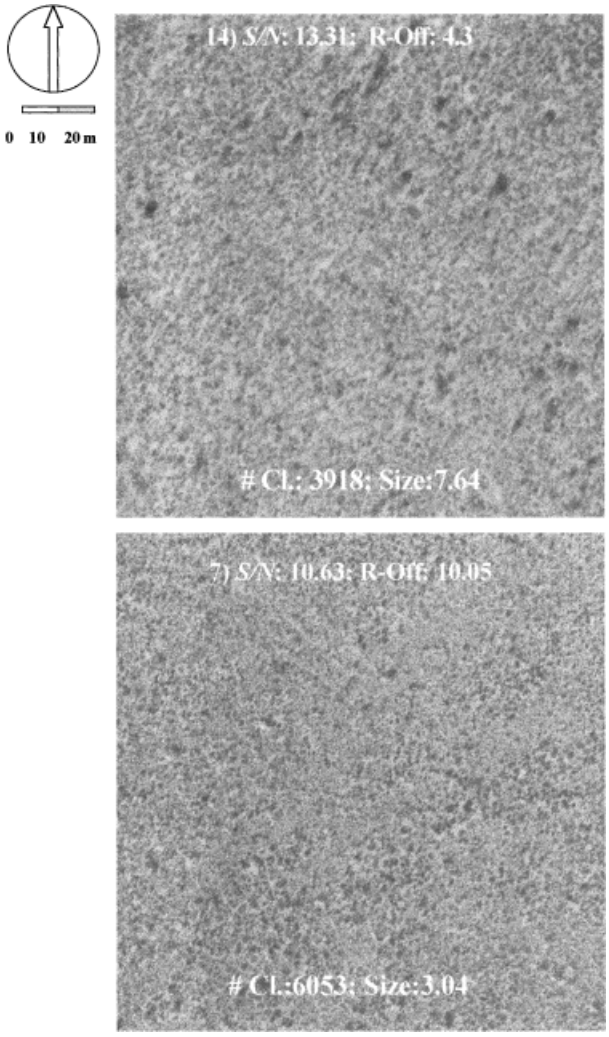


**Fig. 6** Aerial photographs from areas in position 'Far' diverging in their average runoff condition, estimated average *S/N* and corresponding percolation metrics. Cl: number of clusters; size: average cluster size.

The simulation results with *PATCHGEN* under simulated grazer exclusion are numerically consistent with a diminishing average *S/N* value when the average runoff increases within the range 0–36 mm (Fig. 8). Areas with higher local runoff are colonized by smaller plant volumes (smaller patches), as in Fig. 6. This produces a reduction of average *S/N* values.

*Hypothesis 3: Increasing correlation between spatial pattern (an-isotropy) of plant canopy and wind regime as grazing impact increases*

Figure 9 shows the series of *S/N* ratios of individual transects in photographs at Far (Fig. 9a), Medium (Fig. 9b) and Near (Fig. 9c) positions in relation to the

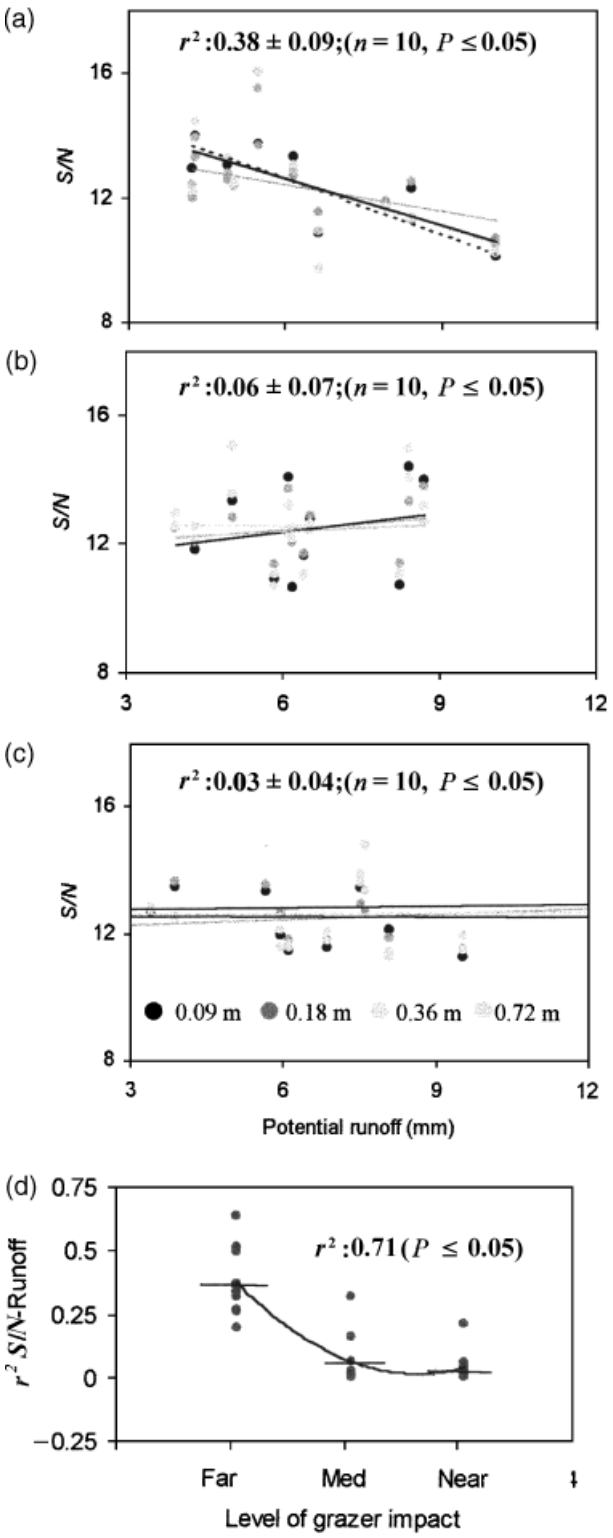


**Fig. 7** (a–c) Linear correlation analysis of average *S/N* vs. average runoff (mm) in images located at Far–Medium–Near positions, respectively, at resolutions from $0.09 \times 0.09$ m to $0.72 \times 0.72$ m; (d) results of Monte Carlo estimates of confidence intervals.

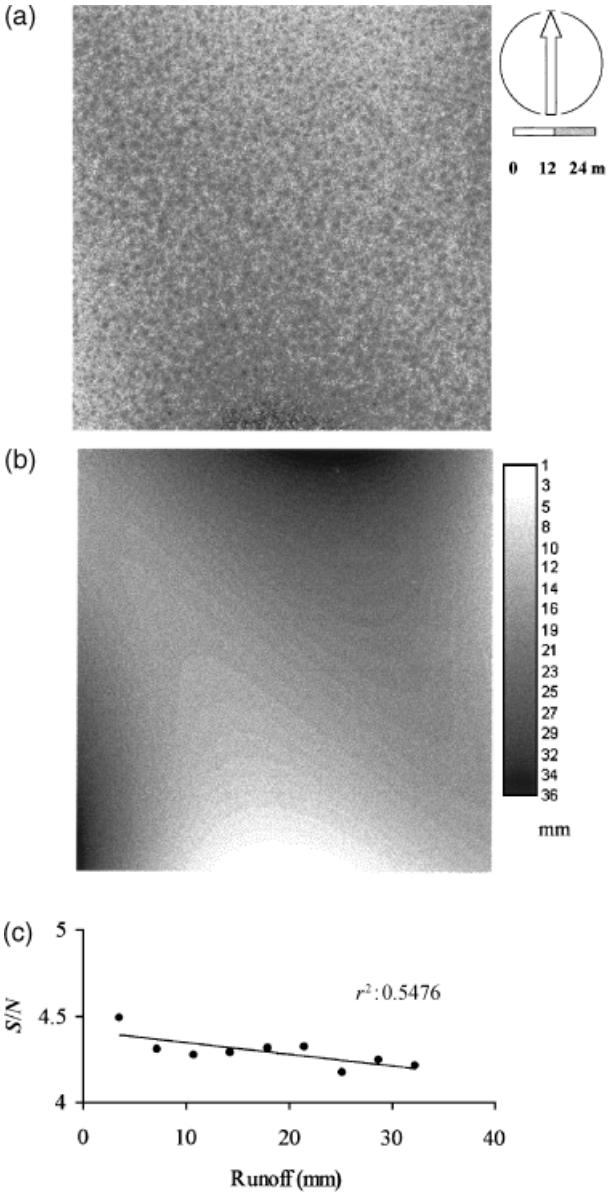


**Fig. 8** (a) Modeled (*PATCHGEN*) nongrazed vegetation canopy corresponding to an area where 0< runoff <36 mm. (b) Spatial runoff pattern corresponding to the same image. (c) Linear correlation in a series of modeled situations with varying average runoff (same spatial pattern as in b).

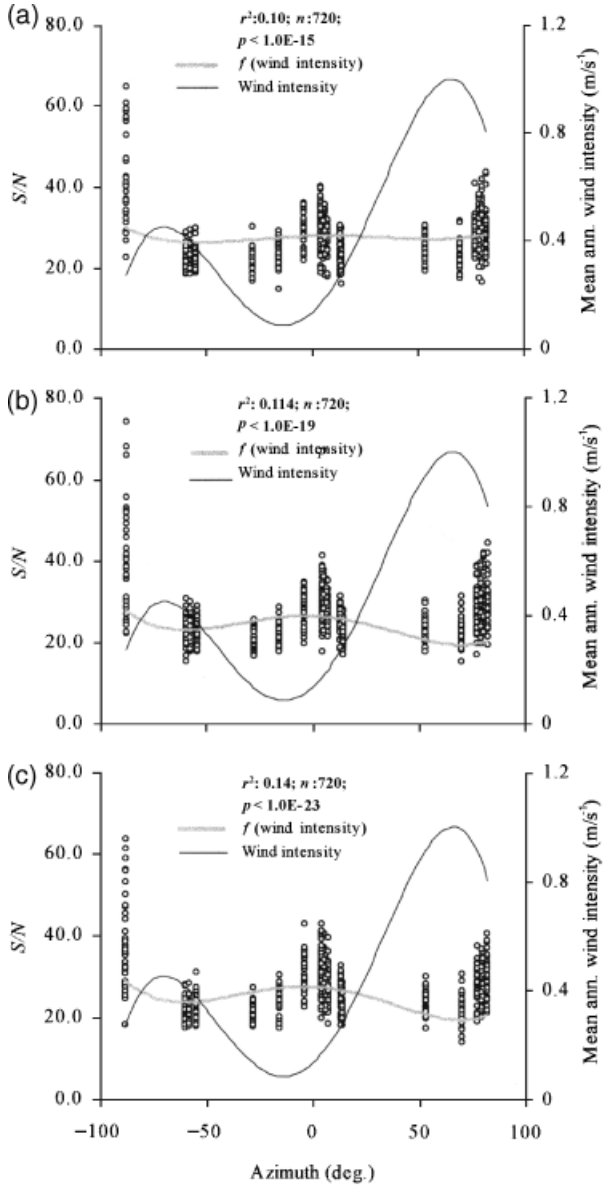


**Fig. 9** An-isotropic distribution of *S/N* transect values as a function of the transect azimuths in photographs at various distances with respect to a single water source. (a) Far; (b) Medium; (c) Near. The wind intensity function *WI* (see also Fig. 3) and a fourth-degree polynomial fitting *f* (*WI*) also shown.

azimuth angle of the transects on which they were calculated. In all three positions with respect to the water source, a model with extremely low probability of rejection is obtained (1E-15 to 1E-23). The squared correlation coefficient (amount of variance accounted by *f* (*WI*) in the joint model with *f* (*A*)) increases from 0.10 at 'Far' position to 0.114 at 'Medium', to 0.14 at 'Near', or 50%, 55% and 77% of the variance explained by the joint model (not shown). *S/N* values are lower at azimuth values where *WI* is higher (and lower *WI* match local high *S/N* values) and these correspondences increase at increasing grazing pressure. Based on these results, we do not find reasons to reject the hypothesis that a wind-related component of plant canopy an-isotropy increases at increasing grazing impact.

Simulations with *PATCHGEN* are consistent with these trends. Figure 10 shows the results of testing an isotropic version of the model (diffusive net growth rates equal in all directions) and two levels of

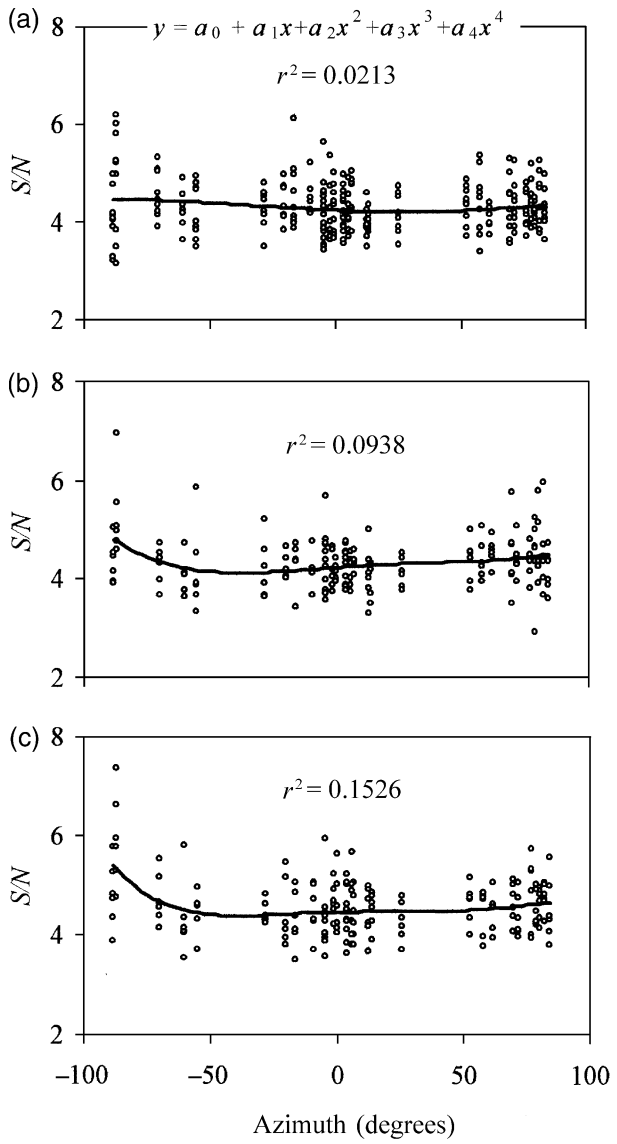


**Fig. 10** *S/N* values corresponding to transects with different orientation to sample output images generated with *PATCHGEN* when introducing increasing degrees of wind-related anisotropy (see also Table 1). (a) Isotropic growth of shrubs assumed. (b) An-isotropic growth of shrubs inversely proportional to predominant *WI*. (c) Same as b, proportionality increased by 3×. The fitting function corresponds to the equation shown in inset a.

an-isotropic growth inversely proportional to the observed *WI* (see Fig. 3). The model generates increasingly an-isotropic images as revealed with correlation analysis. The trend is moderately bi-modal with respect to azimuth, but the inflection points are not so evident as they are in real photographs. This is a consequence of the lower azimuthal resolution of the model in comparison with real images, since spatial anisotropy can only be introduced in the code at 45° intervals due to its basic octet structure (see Table 1). It should be noted that even at its highest level, modeled an-isotropy is not perceptible by visual inspection of the output images (for instance, Fig. 8a). This is, however, also the case in real field photographs (compare with Fig. 6).

## Discussion

The detection and quantification of early desertification changes require the identification of meaningful process-related monitorables (Okin, 2001). We propose describing early desertification in drylands similar to the southern Patagonian Monte in terms of the changes occurring in the spatial structure of the plant canopy in relation with the local runoff and wind regime patterns. The progression of desertification would be characterized by a progressive un-coupling of the plant canopy patterns from the spatial structure of runoff at a landscape scale (>100 m) and simultaneous increasing coupling to the spatial structure of the wind regime. As a monitorable metric for the un-coupling of vegetation from runoff at the landscape scale, we propose the correlation coefficient of average *S/N* of low-altitude photographs with the average potential runoff as estimated from DEMs derived from radar remote sensors (Fig. 7). In order to monitor the progressive coupling of plant patterns with the predominant wind regime, we propose the correlation coefficient of *S/N* values of random-azimuth-oriented transects with a fitting function describing the pattern of predominant wind regime (Fig. 9).

The techniques we present to detect early changes during desertification comply with criteria relative to its practical feasibility, in terms of how many samples are needed to distinguish small, man-made variability on a matrix of natural (eventually large) variability, and whether the needed number of samples can be collected on a periodic basis with a feasible sampling effort. Our results indicate that several thousands of transects (300–500 m long) must be inspected in order to detect early changes of plant structure in an area of about 300 $km^2$. Note that our study involves the analysis of about 12 000 such transects. The photographic material for this analysis was collected during two flight hours and the data processing demanded about 15 man-hour effort. These are probably adequate practical conditions to allow periodic monitoring in most similar dryland areas.

A comment is in order about the reliability of a monitoring strategy based on the above metrics in terms of *precision*, or the ability to detect small structural changes over large areas when they occur. In principle, the precision of the metrics can be made as high as desired by increasing the amount of inspected

transects on the photograph fields. This is achieved by introducing some minor changes in the computer code that processes the digital image files, and involves small increases in computing time. While this should hold in most cases, it can be predicted that the relative success in increasing precision by this means will depend on the natural 'background' variability in the inspected area.

*Self-consistency*, or the ability of obtaining similar estimates at places that do not change over time, is another dimension of reliability. This depends on various factors related to the flying equipment used, the prevailing meteorological conditions during flight time and the skill of the operators in handling the camera and geo-positioning equipment. Strong winds might prevent maintaining a desired flying route within the precision attained in this study. Since plant shadows can introduce false plant anisotropy particularly at low solar elevation angles, care should be taken in selecting flying times when plant shadows are not elongated in the direction of predominant winds, but nearly orthogonal to them. Under these latter conditions, solar anisotropy can be effectively out-filtered from wind anisotropy, as done in this study.

It should be noted that the presence of small (anthropic-related) sources of variation in a frame of large naturally occurring variability results in low values of the estimated correlation coefficient attributable to the anthropic-related source. However, the corresponding probability at which the null hypothesis can be rejected can be made notoriously low by increasing the amount of data points. (see Figs 9 and 10).

In the Patagonian Monte and similar systems, the inter-annual variability of rainfall is extremely high (Barros & Rivero, 1982). This complicates the design of monitoring systems to detect nonseasonal changes in time, because even observations performed at the same date (say every year) can show large fluctuations due to temporal modifications of the plant canopy after rain events. It is our view that monitoring *structural* changes would necessarily be more convenient than monitoring *floristic* changes, or surrogate estimates thereof depending on the plant canopy-soil reflectance or the green intensity of plant canopy color (like in usual satellite imagery). Structural changes in semiarid shrublands basically depend on the location and size of long-lived shrubs, which act as spatial organizers of other life forms around them. Shrub size varies little (and shrub position might not vary at all) during temporary droughts or humid periods or seasons because they are rooted deeper than grasses and can better tap soil water reserves. Accordingly, we hypothesize that indicators derived from the spatial arrangement and size of shrubs can be expected to show considerably lesser temporal variation than those based on seasonally fluctuating herbaceous forms, while still embedding process-meaningful signals of the state of the shrubland system. .

In the conception of Schlesinger *et al.* (1996), an increase in the heterogeneity of water, nitrogen and other soil resources occurs during progressing desertification. Our data along grazing gradients in the Patagonian Monte indicate that the structural variability of the plant canopy is reduced at scales of 200–300 m as the grazing intensity increases. These changes are coupled to the distribution of shrubs and perennial grasses. These life forms tend to create, maintain and be influenced by localized soil microsites with characteristic chemical and physical conditions beneath and around them (Mazzarino *et al*., 1996; del Valle & Rosell, 1999; Carrera *et al*., 2000). The impact of domestic grazing reduces the shrub size and internal cover of shrub-dominated patches in the Patagonian Monte. The soil moisture vary inside and outside the patches depending on their size and internal cover, as shown by micrometeorological field measurements, and these trends alter the sheltering-competition balance between shrubs and grasses (Bertiller *et al*., 2002a). These trends prompt interest in developing clues to interpret changes in the spatial pattern of plant canopies as early indicators of dryland degradation.

In a previous paper (Ares *et al*., 2003a), we showed that the *S*/*N* ratio decreases in areas severely impacted by grazing, because shrub patches are disrupted and spatially disorganized into smaller units, fragments of remnant patches, etc. In this study, where early stages of desertification were observed, the average *S*/*N* ratios do not diminish significantly with increasing grazing impact, but their frequency distribution shifts significantly towards a reduced frequency of low values and an increased frequency of central values. These trends are consistent with an increasing shrub encroachment, as reported for similar shrublands (Beeskow *et al*., 1995; Klausmeier, 1999). The examples shown in Fig. 11 indicate that the *S*/*N* ratio can be used to characterize the spatial structure of the plant canopy in relation with these changes. Figure 11a and b shows that the *S*/*N* metric can quantify the degree of heterogeneity of a spatial distribution in comparison with that of a theoretically random one. Figure 11c–f shows that the *S*/*N* ratio also quantifies the contrast between emerging structures (shrubs, low trees) with respect to a background of lower structures like those corresponding to perennial grass tussocks.

Several authors have analyzed the interactions between the runoff and the vegetation pattern in drylands. The occurrence of linear surface flow when

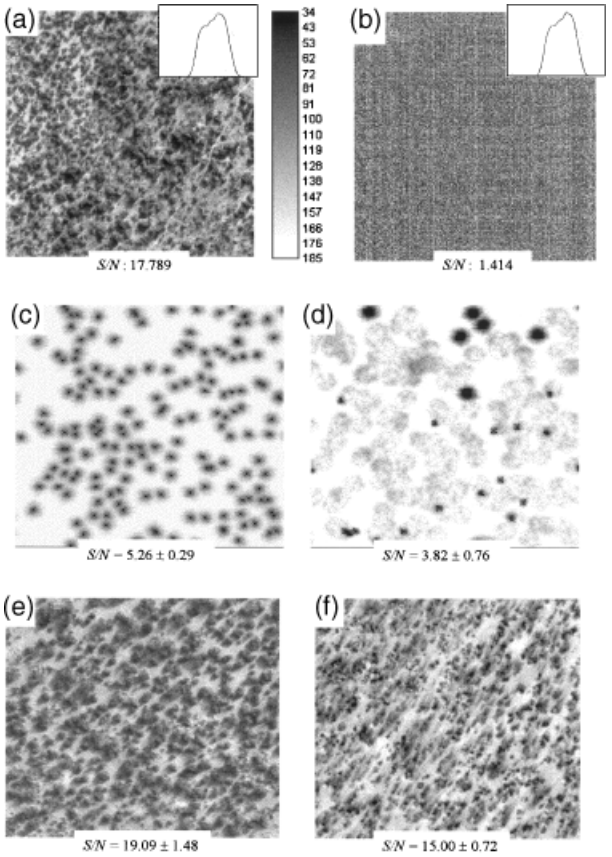


**Fig. 11** Real and modeled images of spatial plant distribution that illustrate the meaning of the *S/N* metric.

rainfall exceeds a certain threshold tends to limit the development of banded patterns and favor the formation of dotted bush. These trends have been observed in Niger (Leprun 1999; Valentin & d'Herbès 1999), in Mediterranean semiarid conditions (Bergkamp *et al*., 1999) and in semiarid and arid areas of Australia (Tongway & Ludwig, 1990; Dunkerley & Brown, 1999). Our results show that the average *S/N* value diminishes as the average runoff increases in relatively undisturbed land conditions ('Far' from water sources). In our case, the range of changes related to runoff does not involve a transition from banded to spotted patterns, but a change in the grain of these latter. Both the visual inspection of the photographs as well as the analysis of selected cases with percolation metrics (Milne *et al*., 1999) indicate that most of the reduction in *S/N* values can be traced back to a reduction in individual patch sizes. Calculations with *PATCHGEN* using a simulated runoff grid (Fig. 8) and assuming runoff-dependent sizes of shrubs and grasses are numerically consistent with this interpretation. A mechanistic explanation of the effect of runoff in limiting plant size would imply a reduction of the carrying capacity at areas with high runoff because of enhanced nutrient washout, as observed in experiments at similar shrublands with controlled conditions (Schlesinger *et al*., 1999).

Domestic grazing disrupts the functional relations between runoff and plant canopy patterns. The perennial grasses interspersed among shrubs in a mulga woodland (Anderson & Hodgkinson, 1997) were adversely affected by grazing, reducing the capacity of the vegetation canopy to capture runoff water and nutrients and affecting the mulga-banding. Wu *et al*. (2000) found that vegetation bands in Niger were seriously affected during the period 1960–1992 by human-managed herbivores. Montaña *et al*. (2001) suggested that adequate monitoring of band integrity needs to be developed in order to provide early warnings of land degradation. In this study, we show that the spatial spotted pattern of vegetation canopy is progressively un-coupled from the pattern of natural runoff in areas with increasing grazing impact. Grazing effects on the plant canopy structure override those resulting from the landscape runoff pattern.

In a previous paper where we performed long-term monitoring of the amounts of flying soil dust at the Patagonian Monte (Ares *et al*., 1990), we showed that the generation of soil dust is increasingly related to wind intensity as the total vegetation cover decreases. Okin (2001) summarized current ideas about the possible effects of wind on modifying plant spatial patterns in semiarid shrublands. These include increased saltation of sand grains and sand-blasting of plants, increased plant evapotranspiration and increased winnowing of fine particles leading to decreased water-holding capacity. All these effects can be expected to be more intense at the windward side of shrub patches than at the leeward side of them. As a consequence of these, the net growth of plant parts can be expected to be greater at the lee-side of shrubs (this would include both the local growth of established plants as well as that from colonizers finding sheltered microsites at downwind orientations). In our study, wind-oriented anisotropy of plant volumes is a minor trait accounting for 10–14% of the variance of *S/N* records in random-oriented transects. However, intensive spatial sampling shows that there is a significant increasing correlation trend with increasing grazing impact. Numerical simulation with *PATCHGEN* indicates that increasing the shrub growth rate in proportion to the directions of predominant winds creates spatial anisotropy having characteristics similar to those observed in real field images. It should be mentioned that a modeled 3 × inverse proportionality of growth rates to wind intensities creates anisotropy that is detectable with statistical techniques (Fig. 10), but is not evident to the naked eye, nor with the limited

sampling intensity feasible in field observations at ground level (A. Bisigato, unpublished results).

## Conclusions

Early stages of desertification can be identified in shrublands of the Patagonian Monte through the analysis of changes in the spatial distribution of the plant canopy. The observed changes can be interpreted in terms of a progressive un-coupling of the vegetation pattern from that of the runoff at a landscape scale, and a simultaneous and progressive relation with the prevailing wind regime. High-resolution aerial photographs and Digital Elevation Models derived from radar remote imagery can be used to investigate runoff un-coupling, while the analysis of image an-isotropy can be used to detect predominant wind effects along grazing gradients. Fourier-based metrics can be used in both cases, and the techniques can probably be applied at a scale adequate for regular monitoring and surveillance of other extended shrublands in the world.

## Acknowledgements

Dr M. Bertiller contributed with ideas and comments at various stages of the study. Dr C. Ibarra provided technical assistance in developing the flight procedures and protocols. Funds were supplied by Agencia Nacional de Promoción Científica y Tecnológica (FONCYT), Project BID 1201/OC-AR PICT-99 #08-06027 and GTZ-Universität München-CENPAT-UNPSJB, 'Erfassung und Abschätzung von Desertifikationserscheinigungen in Patagonien'. Interferometric techniques for the calculation of the DEM of the study area were made available for the scope of this project by the Remote Sensing Data Center (DFD) of the German Aerospace Center (DLR). Special thanks are due to A. Roth for software support. The European Space Agency (ESA), DLR and Comisión Nacional de Actividades Espaciales (CONAE) from Argentina supplied the satellite images. A patient anonymous reviewer made detailed and critical comments that contributed to the improvement in the presentation of our results.

## References

Adler PB, Raff DA, Lauenroth WK (2001) The effect of grazing on the spatial heterogeneity of vegetation. *Oecologia*, **128**, 465–479.

Anderson VJ, Hodgkinson KC (1997) Grass-mediated capture of resource flows and the maintenance of banded mulga in a semi-arid woodland. *Australian Journal of Botany*, **45**, 331–342.

Ares JO, Beeskow AM, Bertiller MB, *et al*. (1990) Structural and dynamic characteristics of overgrazed grasslands in northern Patagonia. In: *Managed Grasslands. Regional Studies* (ed. Breymeyer A), pp. 268–274. Elsevier, Amsterdam.

Ares J, Bertiller M, Bisigato A (2003a) Modeling and measurement of structural changes at a landscape scale in dryland areas. *Ecological Modeling and Assesment*, **8**, 1–13.

Ares J, Bertiller M, Bisigato A (2003b) Estimates of dryland degradation with Fourier signatures in low-altitude high resolution monochromatic images. *Landscape Ecology*, **18**, 51–63.

Baker WL (1989) A review of models of landscape change. *Landscape Ecology*, **2**, 111–133.

Barros V, Rivero M (1982) Mapas de probabilidad de la precipitación en la provincia de Chubut. National Patayonic Center, Puerto Madryn.

Beeskow AM, Elissalde NO, Rostagno MC (1995) Ecosystem changes associated with grazing intensity on the Punta Ninfas rangelands of Patagonia, Argentina. *Journal of Range Management*, **48**, 517–522.

Bergkamp G, Cerdà A, Imeson AC (1999) Magnitude-frequency analysis of water redistribution along a climate gradient in Spain. *Catena*, **37**, 129–146.

Bertiller MB, Sain CL, Bisigato AJ *et al*. (2002a) Spatial sex segregation in the dioecious grass *Poa ligularis* in northern Patagonia: the role of environmental patchiness. *Biodiversity and Conservation*, **11**, 69–84.

Bertiller MB, Ares J, Bisigato A (2002b) Multiscale indicators of land degradation in the Patagonian Monte, Argentina. *Environmental Management*, **30**, 704–715.

Bisigato AJ, Bertiller MB (1997) Grazing effects on patchy dryland vegetation in northern Patagonia. *Journal of Arid Environments*, **36**, 639–653.

Bisigato A, Ares J, Bertiller M (2002) Assessment of pristine vegetation structure in semiarid shrublands based on spatial explicit modelling. *Phytocoenologia*, **32**, 581–594.

Bloomfield P (1976) *Fourier Analysis of Time series: An Introduction*. John Wiley, New York.

Brown MA, Waller SS (1986) The impact of experimental design on the application of grazing research results – an exposition. *Journal of Range Management*, **39**, 197–200.

Busso CA (1997) Towards an increased and sustainable production in semiarid rangelands of central Argentina: two decades of research. *Journal of Arid Environments*, **36**, 197–210.

Carrera AL, Sain CL, Bertiller MB (2000) Patterns of nitrogen conservation in shrubs and grasses in the Patagonian Monte, Argentina. *Plant and Soil*, **224**, 185–193.

Coulson SN (1995) SAR interferometry. In: Multi-Disciplinary Online Documentation. URL: http://earth.esa.int/docpot.

Couteron P, Lejeune O (2001) Periodic spotted patterns in semiarid vegetation explained by a propagation-inhibition model. *Journal of Ecology*, **89**, 616–628.

Crow EL, Davis FA, Maxfield M (1993) *Statistics Manual*. Dover Pulications Inc., New York.

Defossé GE, Bertiller MB, Rostagno C (1992) Rangeland management in Patagonian drylands. In: *Proceedings of the International Rangeland Development Symposium* (eds Perrier GK, Gay CW), pp. 12–21. Society for Range Management, Spokane.

Delhoumme JP (1996) Fonctionnement hydropédologique d'une toposequence de sols an milieu aride (reserve de la biophère de Mapimi, Nord-Mexique). PhD Thesis, Université de Poitiers, Poitiers.

del Valle HF, Rosell A (1999) Formation, distribution and physicochemical properties of plant litter in shrub patches of northeastern Patagonia. *Arid Soil Research and Rehabilitation*, **13**, 105–122.

del Valle HF, Buck A, Mehl H (2002) Digital elevation models as tools in soil research in northeastern Patagonia. In: *XVIII Argentine Soil Science Meeting*, Puerto Madryn (Chubut), Argentina, 16–19 April 2002, p. 112 (abstracts).

Dunkerley DL (1997) Banded vegetation: survival under drought and grazing pressure based on a simple cellular automaton model. *Journal of Arid Environments*, **35**, 419–428.

Dunkerley DL, Brown KJ (1999) Banded vegetation near Broken Hill, Australia: significance of surface roughness and soil physical properties. *Catena*, **37**, 197–216.

Galle S, Ehrman M, Peugeot C (1999) Water balance on a banded vegetation pattern. A case study of tiger bush in western Niger. *Catena*, **37**, 197–216.

Greene RSB, Ringrose-Voase AJ (1994) Micromorphological and hydraulic properties of surface crusts formed on a red earth soil in the semiarid rangelands. In: *Proceedings of the IX International Working Meeting on Soil Micromorphology* (eds Ringrose-Voase AJ, Humpheys GS), pp. 763–776. Elsevier Science Publishers, Amsterdam.

Holm A, Loneragan WA, Adams MA (2001) Do variations on a model of landscape function assist in interpreting the growth response of vegetation to rainfall in arid environments? *Journal of Arid Environments*, **50**, 23–52.

Hudak AT, Wessman CA (1998) Textural analysis of historical aerial photography to characterize woody plant encroachment in South African savanna. *Remote Sensing of the Environment*, **66**, 317–330.

Jenson S, Domingue J (1988) Extracting topographic structure from digital elevation data for geographic information system analysis. *Photogrammetric Engineering and Remote Sensing*, **54**, 1593–1600.

Klausmeier CA (1999) Regular and irregular patterns in semiarid vegetation. *Science*, **284**, 1826–1828.

Landsberg J, James CD, Maconochie J *et al*. (2002) Scale-related effects of grazing on native plant communities in an arid rangeland region of South Australia. *Journal of Applied Ecology*, **39**, 427–444.

Le Houérou HN, Bingham RL, Skerbek L (1988) Relationship between the variability of annual precipitation in world arid lands. *Journal of Arid Environments*, **15**, 1–18.

León RJC, Bran D, Collantes M *et al*. (1998) Grandes unidades de la Patagonia extra andina. *Ecología Austral*, **8**, 125–144.

Leprun JC (1999) The influences of ecological factors on tiger bush and dotted bush patterns along a gradient from Mali to northern Burkina Faso. *Catena*, **37**, 25–44.

Mares MA, Morello J, Goldstein G (1985) The Monte desert and other subtropical semi-arid biomes of Argentina, with comments on their relation to North American arid areas. In: *Hot Deserts and Arid Shrublands, Ecosystems of the World*, **Vol 12** (eds Evenari M, Noy-Meir I, Goodall D), pp. 203–237. Elsevier Science, Amsterdam.

Mazzarino MJ, Bertiller MB, Sain CL, Laos F, Coronato F (1996) Spatial patterns of nitrogen availability, mineralization and immobilization in northern Patagonia (Argentina). *Arid Soil Research and Rehabilitation*, **10**, 295–309.

Milne BT, Johnson AR, Matyk S (1999) Clara-T: Instructional software for fractal pattern generation and analysis. In: *Landscape Ecological Analysis* (eds Klopatek JM, Gardner RH), pp. 304–332. Springer-Verlag, New York.

Montaña C, Seghieri J, Cornet A (2001) Vegetation dynamics: recruitment and regeneration in two-phase mosaics. In: *Banded Vegetation Patterns in Arid and Semiarid Environments* (eds Tongway DJ Valentin C, Seghieri J), pp. 132–145. Springer-Verlag, New York.

OIES (1991) *Arid Ecosystem Interactions*. Office of Interdisciplinary Earth Studies, Boulder, CO, USA, 81 pp.

Okin GS (2001) Wind-driven desertification: process modeling, remote monitoring and forecasting. PhD Thesis, California Institute of Technology, California, 269 pp.

Parizek B, Rostagno CM, Sottini R (2002) Soil erosion as affected by shrub encroachment in north-eastern Patagonia. *Journal of Range Management*, **55**, 43–48.

Pickup G, Chewings VH, Nelson DJ (1993) Estimating changes in vegetation cover over time in arid areas from remotely sensed data. *Remote Sensing of the Environment*, **43**, 243–263.

Pickup G, Bastin GN, Chewings VH (1998) Identifying trends in land degradation in non-equilibrium rangelands. *Journal of Applied Ecology*, **35**, 365–377.

Reynolds JF, Fernández RJ, Kemp PR (2000) Drylands and global change: rainfall variability and sustainable rangeland production. In: *Proceedings of the 12th Toyota Conference: Challenge of Plant and Agricultural Sciences to the Crisis of Biosphere on the Earth in the 21st Century* (eds Watanabe K, Komamine A), Toyota Motor Co., Mikkabi, Shizuoka, Japan.

Schlesinger WH, Reynolds JF, Cunningham GL, Huenecke LF, Jarrel WM, Virginia RA, Whitford WG (1990) Biological feedbacks in global desertification. *Science*, **247**, 1043–1048.

Schlesinger WH, Raikes JA, Hartley AE, Cross AF (1996) On the spatial pattern of soil nutrients in desert ecosystems. *Ecology*, **77**, 364–374.

Schlesinger WH, Abrahams AD, Parsons AJ, Wainwright J (1999) Nutrient losses in runoff from grassland and shrubland habitats in Southern New Mexico: I. rainfall simulation experiments. *Biogeochemistry*, **45**, 21–34.

Sharifi M, Gibson A, Rundel P (1999) Phenological and physiological responses of heavily dusted creosote bush (*Larrea tridentata*) to summer irrigation in the Mojave Desert. *Flora*, **194**, 369–378.

Tongway DJ, Ludwig JA (1990) Vegetation and soil patterning in semiarid mulga lands of eastern Australia. *Australian Journal of Ecology*, **15**, 23–34.

Valentin C, d'Herbès JM (1999) Soil and water components of banded vegetation patterns. *Catena*, **37**, 1–24.

Wester DB (1992) Viewpoint: replication, randomization, and statistics in range research. *Journal of Range Management*, **45**, 285–290.

Wiegand T, Milton SJ, Wissel C (1995) A simulation model for a shrub ecosystem in the semiarid Karoo, South Africa. *Ecology*, **76**, 2205–2221.

Wu XB, Thurow TL, Whisenant SG (2000) Fragmentation and functional change of tiger bush landscapes in Niger. *Journal of Ecology*, **88**, 790–800.

## Appendix I

The *S/N* metric is an application of Fourier spectral analysis to the description of the spatial distribution of a scalable attribute. Take for example, a vector $X$ of $x_1, x_2, \ldots, x_n$ values representing the local biomass of a plant species in laterally contiguous quadrants of side size $l$ along a line transect of length $l \times n$, $n \gg l$. It can be shown that all $x_i$ values can be expressed as a sum of sine and cosine functions $<$of the type

$$x_l = A_0 + \sum_{0<j<n/2} (A_j \cos \omega_j l + B_j \sin \omega_j l) + (-1)^l A_{n/2},$$

where the $\omega_j$ are the Fourier frequencies at length $l$, and the coefficients $A_0$, $A_j$, $B_j$, $A_{n/2}$, correspond to the mean, the relative contribution of each frequency to the description of the series $x_l$ and their phases, respectively. The coefficients are computed (Bloomfield 1976) in the frequency domain through the Fast Fourier Transform algorithm, which yields the partial contribution or magnitude $M$ (sum of cosine and sin terms at each frequency) of all harmonics in describing the data series.

In characterizing the sets of Fourier magnitudes we used the ratios of the cumulative magnitudes at low frequencies in relation to those at high frequencies (*S/N* ratios):

$$S/N = \Sigma_{M_l} / \Sigma_{M_h},$$

where $M_l$ and $M_h$ are the magnitudes at user-specified ranges of low (signal) and high (noise) frequencies. In this contribution, we used the ratio defined at $\Sigma_{M0–0.25}/\Sigma_{M0.26–0.5}$, the lower and higher half frequency ranges, respectively. In terms of the vegetation canopy, the 'signal' refers to the degree of development of patch structures and their spatial arrangements, while the 'noise' refers to the distribution of nonpatchy structures like fragments of old patches, randomly located colonizers, etc. Homogeneous patch growth creates low-frequency variation (*S/N* ratio increases), while heterogeneous patch development, fragmentation into smaller units, etc. creates high-frequency variation, which is reflected in decreased $S/N$ ratios.

An intuitive perception of the meaning and behavior of the *S/N* ratio can be gained by inspecting the set of image examples shown in Fig. 11. In Fig. 11a, an aerial nadir-oriented photograph of a field in the area described in this study is shown. The image has been digitized to a resolution of 1024 rows × 1024 columns, or $1024^2$ pixels, and associated to a 256-grade gray-palette. These translate every value in the image to a gray-tone scale, as described in the vertical bar along the right side of the photo. The frequency distribution of all pixel values is outlined in the small upper-right inset. A relatively high average *S/N* ratio corresponding to 20 randomly oriented transects sampling optical density in this image reflects the occurrence of well-defined spatial structures (clumps of high optical density corresponding to vegetation patches contrasting with their background). Figure 11b shows the same image after a process of randomization, i.e. a computer code mixed image columns and rows just like card players do before each game. Although the range of values contained in the image is the same as in Fig. 11a (they have identical frequency histograms), the spatial distribution is deployed of any structural arrangement. Note that the *S/N* ratio approaches 1, meaning that these are the same magnitudes associated with signals (patches) as with noise (background).

Consider now Fig. 11c. This represents the spatial distribution of a single un-grazed plant form, generated by a stochastic simulation model (Ares *et al.*, 2003a). Although patches are randomly distributed over the surface, they have a similar size and geometric structure. Each patch corresponds to a group of contiguous pixels in the image, with ascending and descending values around a central maximum. The average *S/N* describing this structure is 5.26 ($\pm$0.29, $P < 0.05$), where the confidence interval corresponds to the mean of 5 random realizations of the model. In Fig. 11d, grazing on the same plant canopy has been simulated. The herbivore has consumed the fastest growing portions of plant patches down to a given threshold. Because of herbivore selection, some patches remain undamaged and attain a large size, while others are confined to a small size. Also, newly formed patches appear as small dots scattered on the image. This relatively less organized and heterogeneous structure is characterized by a lower $S/N = 3.82$ ($\pm$0.76, $P < 0.05$).

Consider now Fig. 11e–f. These correspond to photographs of study areas presented in this paper differing in grazing intensity as estimated by their distance to a single water source (4000–5000 m, low grazing intensity, Fig. 11e) and a site near a water source ($<$1000 m, high grazing intensity, Fig. 11f), respectively. The intensively grazed area shows a spatial arrangement of plant patches with increased randomness and size heterogeneity as compared with the less intensively grazed area.

The *S/N* ratio estimated on data obtained in 'ground truth' field transects has been shown (Bertiller *et al.*, 2002b) to be quantitatively related to the density of patches ($D$), the size (radius $R$) of the patches and the internal cover ($C$) of the patch units. ($S/N = -2.28D + 3.14R + 4.10C$, $r^2 = 0.98$, $P \leq 0.001$).